S275JR Mild Steel Corrosion Sites Deactivation in Sodium Sesquicarbonate Heavy Deposits Using Piperaquine as Alternative Inhibitor

B. U. Ugi[1*], V. M. Bassey[1], P. B. Ashishie[1], D. O. Nandi[1] and F. B. Ugi[2]

[1]*Department of Pure and Applied Chemistry, Faculty of Physical Sciences, University of Calabar, P. O. Box 1115, Nigeria*
.[2]*Chemical/Petrochemical Engineering Department, Rivers State University, Port Harcourt, Nigeria*
*Corresponding author: ugibenedict@gmail.com

Received 14/08/2022; accepted 08/11/2022
https://doi.org/10.4152/pea.2024420202

Abstract
This study researched S275JR MS corrosion sites deactivation in [$Na_3H(CO_3)_2$] heavy deposits (Gamboru, Borno State, Nigeria), using PPQ as alternative inhibitor, and employed WL, HER, EIS, PDP, SEM and computational techniques. PPQ showed effective MS corrosion mitigation in [$Na_3H(CO_3)_2$] heavy deposits. IE(%) of 98.8, 99.5, 82.9 and 95.9 %, for gravimetric, HER, EIS and PDP, respectively, at 208 K, were obtained. PPQ had a shortest ΔE of 0.1 eV, with a higher absolute molecular σ of 2.4, compared to molecular η of 0.4, which makes it a better inhibitor of MS corrosion in [$Na_3H(CO_3)_2$] heavy deposits. With higher inhibitor Ct, its IE(%) increase and CR of MS decreased. This was due to PPQ molecules strong adsorption onto the MS surface. PPQ was also thermodynamically stable, showed less disorderliness, and its absorption was spontaneous and physical.

Keywords: adsorption; corrosion; EIS; HOMO; LUMO; [$Na_3H(CO_3)_2$]; physisorption PDP; PPQ; SEM.

Introduction•

The struggle to combat corrosion effects on materials, especially metals, has come a long way regarding the use of different protective measures, especially environmental modifications [1]. Corrosion is an Ec process that occurs at the major corrosion active sites of a material, which predominantly affects anodic areas and some parts of the cathodic ones. It is most likely to occur where moisture, air, electrolytes and possible electron migration from the anodic electrode or sites are present, due to metal dissolution that causes oxidation [1-2]. Literature has proven that continued research on the use of organic phytocompounds for corrosion mitigation lies on their readily availability, low cost, and presence of phytoatoms such as N, Sulphur and P. [1, 3]. Organic CI is based on phytochemicals atoms adsorption onto the surface of a material, usually metal, to

• The abbreviations and symbols definition lists are in page 111.

form a protective film which displaces water from the metal surface and protects it against deterioration [1-4]. S275JR MS is one of the most commonly used grades in general construction. It is an un-alloyed, hot rolled and low C MS [2-3]. S275JR is available in a wide choice of profiles and presentations. It is easy to cut, using appropriate grade cutting disks or flame cleaving methods, weld (without need to preheat the metal) machine and drill, which makes it the perfect choice for frames, vehicles, joist supports, lintels, shelves, brackets, construction and maintenance projects. [2-3]. To obtain best results, the most appropriate specification of welding rods and electrodes for low C MS must be used. For annealing, the piece must be slowly heat from 650 to 700 ºC, and then gradually cooled, preferably in a furnace [2-3]. S275JR is prone to rust. It is important that its surface is treated after fabrication, by using red oxide primer and an appropriate metal paint or spray [2]. PPQ (1.3-bis[4-(7-chloroquinolin-4-yl)-4piperazin-1-yl]-propane) is a member of the 4-aminoquinoline antimalarial group, being structurally related to chloroquine, in which the N at position 4 of the PPQ moieties is replaced by a 7-chloroquinolin-4-yl group. PPQ is an N-arylpiperazine, an organochlorine and an aminoquinoline. It is repurposed as a partner drug in artemisinin-based combination therapy, of each tablet contains 320 mg PPQ (as phosphate). PPQ structure is presented in Fig. 1.

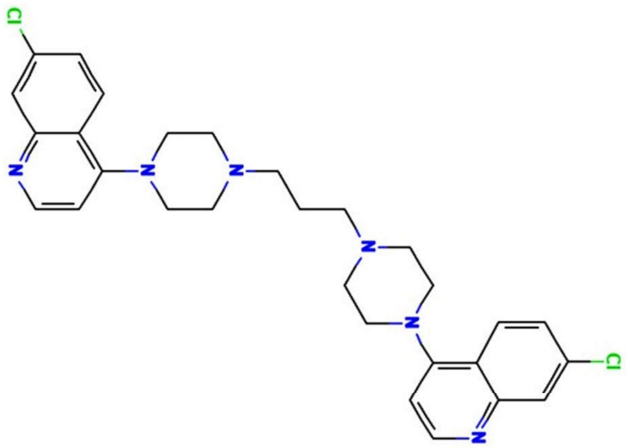

Figure 1: PPQ molecular structure.

In the pursuit for an eco-friendly, readily accessible and inexpensive CI in strong electrolytes, especially those eroding MS in [$Na_3H(CO_3)_2$], the present study assessed PPQ, for understanding its adsorption mechanism, thermodynamic stability, IE(%), T dependency, Ec relations, etc.

Materials and methods

MS and PPQ preparation

The metal employed in this study was S275JR MS obtained from Ibom Metal and Aluminum Company, Akwa Ibom State, Nigeria, with a composition of Fe (97.43%), C (0.2%), Si (0.05%), Mg (1.6%), S (0.05%), K (0.04%) and Cu (0.27%). It was cut into dimensions of 2.5 x 0.1 x 2.5 cm, for WL and HER experiments, and 1 x 1 cm, for Ec methods. MS physical properties are shown in Table 1.

Table 1: S275JR MS physical properties.

Physical property	Value
Density	7800 Kg/m³
Mp	1460 ºC
Elasticity mode	210 GPa
Electrical resistance	0.20-0.25 μΩm
Thermal conductivity	50 W/m°k
Thermal expansion	11 μm/m-k

The resized MS samples were carefully polished to mirror surface, with 220, 800 and 1200 emery grade paper, using a UNIPOL-820 metallographic polishing machine. Then, they were washed with clean water, using a bristle brush, degreased with ethanol and rinsed in acetone, air dried and stored in an air tight 5YHT desiccator containing $CaCl_2$, prior to use.
10 g PPQ were put in a 1000 mL round bottom flask with 5 M [$Na_3H(CO_3)_2$], for 48 h, in order to allow for complete dissolution, and then filtered. Various Ct of PPQ (1.0, 2.5, 4.0, 5.5 and 7.0 g/L) were prepared.

Gravimetric experiment

MS samples, which were initially stored in a desiccator, were removed and rinsed in distilled water, and its initial weight was taken using an ADAM PGW 253e electronic digital balance. They were then immersed in different 100 mL beakers containing the prepared inhibitor in 5 M [$Na_3H(CO_3)_2$], at different Ct (1.0, 2.5, 4.0, 5.5 and 7.0 g/L) (Fig. 2a). The system was closely monitored for 60 min, and the corroded MS samples were removed and washed with clean running water, using a bristle brush, degreased with ethanol and rinsed in acetone, air dried, and then weighed. This process was repeated for another 300 min, at 60 min interval, to allow for variations in MS corrosion reaction. Data generated from WL experiment were used to calculate the CR of MS, and θ and IE(%) of PPQ, using Eqs. 1 and 2.

$$\theta = \frac{ƕr_0 - ƕr_i}{ƕr_0} \quad (1)$$

$$IE\% = \frac{ƕr_0 - ƕr_i}{ƕr_0}\ x\ 100 \quad (2)$$

where $ƕr_0$ and $ƕr_i$ are WL in 1 M [$Na_3H(CO_3)_2$] with and without inhibitor, respectively.

HER experiment

This experiment was conducted using a gasometric (HER) assembly (Fig. 2b). In a two-necked flask containing 5 M [$Na_3H(CO_3)_2$], polished MS was immersed while the stopper from the assembly was cocked. Initial HER volume was recorded, while the flask was immersed in a water bath, at a regulated T of 208 K. The readings from the burette for HER volume due to MS corrosion were taken at every 60 s, for 30 min. This process was repeated for each Ct, at different T (208, 308, 318 and 328 K). Data generated from this experiment were extrapolated, and CR was determined. θ and IE(%) of PPQ were determined from Eqs. 3 and 4.

$$\Theta = \frac{\bar{g}r_0 - \bar{g}r_i}{\bar{g}r_0} \quad (3)$$

$$IE\% = \frac{\bar{g}r_0 - \bar{g}r_i}{\bar{g}r_0}\ x\ 100 \quad (4)$$

where $\bar{g}r_0$ and $\bar{g}r_i$ are WL in 1 M [$Na_3H(CO_3)_2$] with and without PPQ, respectively.

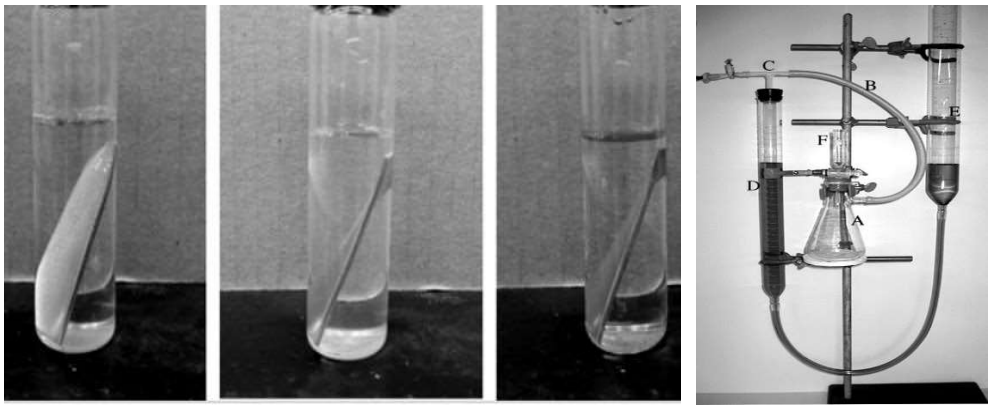

(a) **(b)**

Figure 2: Typical diagrams for **(a)** WL and **(b)** HER experimental assembly.

EIS experiment

EIS test was carried out at 208 K, using a Gamry reference 600 potentiostat/galvanostat with a Gamry framework EIS300 system. Echem Analyst software was used for data analyzing and fitting. The frequency range was from 100 kHz to- 0.01 Hz, and an AC signal amplitude of 10 mV was used. Pt electrode, SCE and S275JR MS were used as CE, RE and WE, respectively. Measurements were performed in an aerated solution, after 30 min (1800 s) immersion in the test solution, at ambient T, in order to attain a steady-state OCP. Nyquist plots derived in PPQ absence and presence were used to obtain some useful kinetic parameters, such as R_{ct}. EI(%) was calculated according to Eq. 5 (Ugi and Obeten, 2019).

$$E\ \% = \frac{R_{cti} - R_{ct0}}{R_{cti}}\ x\ 100 \quad (5)$$

where R_{ct0} and R_{cti} represent R_{ct} without and with PPQ, respectively.

PDP technique

PDP tests were performed at 303 K, using the same instrument as for EIS, and the same data analyzer software. PDP curves were measured at a SR of 0.5 mV/s, from -0.25 to +0.25 V *vs.* SCE. Linear segments of the anodic and cathodic curves were extrapolated from the plots, which gave useful thermodynamic parameters. I_{corr} was used to calculate PPQ IE(%), according to Eq. 6.

$$\mho\ \% = \left[1 - \frac{I^0_{corr}}{I^i_{corr}}\right]\ x\ 100 \quad (6)$$

where $I°_{corr}$ represents I_{corr} obtained without PPQ, respectively (Dagdag et al., 2019).

SEM

SEM, model number JSM-5600 LV, Tokyo, Japan, was used to produce micrographs of MS coupons without and with PPQ in a 1 M HCl solution. The selected coupons were retrieved from the test solution, after 160 h immersion. Each sample was mounted on a metal stub and sputtered with gold. Scanned micrographs were taken at an accelerating V of 1.5 and 12.00 kV. Similar procedure was used by [3].

Result and discussion

Gravimetric analysis results

PPQ IE(%) was assessed through WL procedures. The data obtained through the WL plot of MS in mg, against its IT in the solution with inhibitor, were analyzed, (Table 2). PPQ strength in preventing the of $Na_3H(CO_3)_2$] deposits effect on MS was shown by CR values, which decreased with higher Ct of PPQ. This was due to PPQ strong adsorption onto the MS corrosion active sites [5-9]. IE(%) values of PPQ also proved that it was able to drastically reduce anodic dissolution and cathodic HER [5, 9-10]. Table 2 also shows that θ of PPQ on MS increased with higher Ct. θ explains the exposure area of a material (MS) to an open environment (PPQ). Thus, this trend was to PPQ drastically reduction of MS exposure area to [$Na_3H(CO_3)_2$], hence inhibiting corrosion [4-5, 11].

Table 2: WL results showing CR, θ and IE(%) data.

System (g/L)	CR (mg/cm^2/h)	θ	IE(%)
Blank	1.099	-	-
1.0	0.115	0.896	89.5
2.5	0.055	0.940	94.9
4.0	0.031	0.972	97.2
5.5	0.016	0.985	98.5
7.0	0.013	0.988	98.8

Gasometric experiment

Regarding T effect on PPQ action, Table 3 shows gasometric data.

Table 3: Values of CR (cm^2/min), θ and IE(%)drawn from gasometric analysis.

	208 K			308 K			318 K			328 K		
C (g/L)	CR (cm^2/min)	θ	IE(%)	CR (cm^2/min)	θ	IE(%)	CR (cm^2/min)	θ	IE(%)	CR (cm^2/min)	θ	IE(%)
Blank	1.122	-	-	1.407	-	-	2.091	-	-	3.215	-	-
1.0	0.133	0.889	88.9	0.281	0.800	80.0	0.482	0.769	76.9	1.061	0.669	66.9
2.5	0.093	0.925	92.5	0.260	0.815	81.5	0.457	0.781	78.1	0.901	0.719	71.9
4.0	0.059	0.956	95.6	0.117	0.917	91.7	0.364	0.826	82.6	0.832	0.741	74.1
5.5	0.025	0.986	98.6	0.071	0.949	94.9	0.339	0.838	83.8	0.788	0.755	75.5
7.0	0.016	0.995	99.5	0.034	0.976	97.6	0.101	0.952	95.2	0.479	0.851	85.1

CR results indicate PPQ physical adsorption onto MS, at ambient T (208 K) [10, 12-13]. The decrease in IE(%) with higher T, and correspondent increase in CR of MS, as seen in Table 3, not only indicate physical adsorption, but also explain the possible losing of weakly bonded PPQ molecules, due to the heat effect [13-15].

The desorption process shows that, although PPQ still inhibited MS surface corrosion at higher T, its IE(%) was higher at lower T. This was also due to the inhibitor molecules stronger adsorption onto the MS surface, where CR was minimal [7, 10, 16].

Ec results (EIS and PDP)

Fig. 3a describes Nyquist plot obtained from EIS technique. It shows larger semicircles of high frequency loops, with an increase in PPQ Ct.

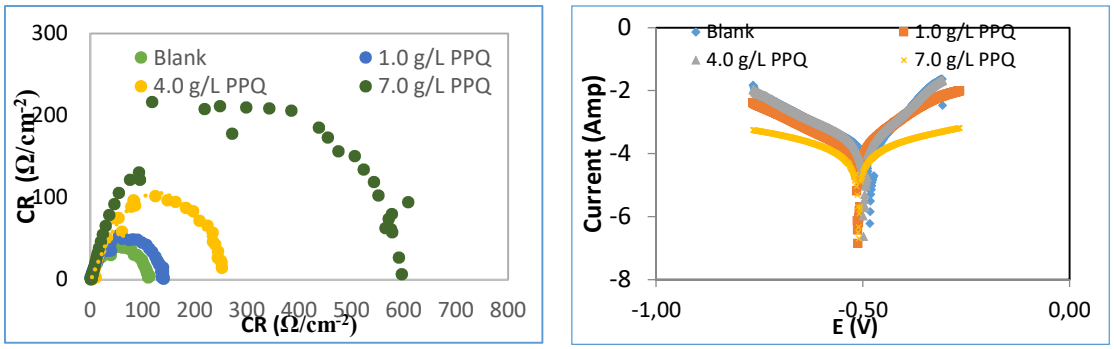

Figure 3: Graphical representation of: **(a)** Nyquist, **(b)** circuit and **(c)** Tafel plots, for Ec determination.

This implies that $[Na_3H(CO_3)_2]$ effect on MS was overcome by PPQ strong adsorption onto the metal corrosion active sites [15-17]. IE (%) data were determined by Eq. 7.

$$\% \wp = \frac{R_{ct}^{0} - R_{ct}^{i}}{R_{ct}^{0}} x\ 100 \qquad (7)$$

where r_{ct}^{0} and r_{ct}^{i} correspond to R_{ct} values in $[Na_3H(CO_3)_2]$ with and without PPQ, respectively.

R_{ct} increased with higher Ct of PPQ (Table 4). More often than not, R_{ct} describes the resistance against the process of electrons transfer from one phase to another. From this result, it was confirmed that electrons transfer from MS anodic sites was retarded by PPQ molecules adsorption onto the metal surface, thus decreasing CR and increasing IE(%) [9, 17].

Table 4: Values of Ec result from EIS and PDP data.

C (g/L)	R_{ct} (Ω/cm^{-2})	C_{dl} ($\mu F/cm^{-2}$)	IE_{Rct}(%)	I_{corr} ($\mu A/cm^{-2}$)	β_a (mV/dec)	β_c (mV/dec)	IE_{PDP}(%)
Blank	104	1.2×10^{-5}	-	2.913	633	711	-
1.0	152	1.9×10^{-6}	31.6	1.046	362	682	64.1
4.0	294	1.1×10^{-6}	64.6	0.872	173	552	70.1
7.0	609	0.9×10^{-6}	82.9	0.118	98	319	95.9

The tendency to store charges by an electrode during an Ec process like corrosion was also considered. Obtained values show a decrease in C_{dl}, which indicates that

PPQ separated the electronic and electrolytic charges at the MS-solution interface. This, in turn, reduced the tendency to store charges, hence enabling CI [18-20]. Fig. 3b reveals Tafel plots for PDP analysis. The plots show divergence towards anode and cathode sites, which implies that PPQ had a mixed type behavior, just as for β_a and β_c values (Table 4) [18, 20]. However, values obtained in Table 4 show that i_{corr} values decreased, while IE(%) increased. This implies that the current produced in the Ec cell decreased while corrosion was occurring [8, 12, 21], due to PPQ molecules strong adsorption onto the anodic sites, which halted electrons transfer from the anode to the cathode, as Ct increased [12].

Quantum chemical calculations

In order to confirm the chemical data and inferences, Ec analyses were conducted. The following parameters were calculated (Eqs. 8 to 12), using the output generated from E_{HOMO}, E_{LUMO}, IP, EA, χ, η, σ, ω and δ, according to [2] and [22].

$$\chi = \frac{IP + EA}{2} \quad (8)$$

$$\eta = \frac{IP - EA}{2} \quad (9)$$

$$\sigma = \frac{1}{\eta} \quad (10)$$

$$\omega = \frac{\chi 2}{2\eta} \quad (11)$$

$$\delta = \frac{1}{\omega} \quad (12)$$

The computational information showing optimized structures, HOMO, LUMO, ω, δ and radial functions for PPQ, is shown in Fig. 4, and the corresponding calculated data are shown in Table 5.

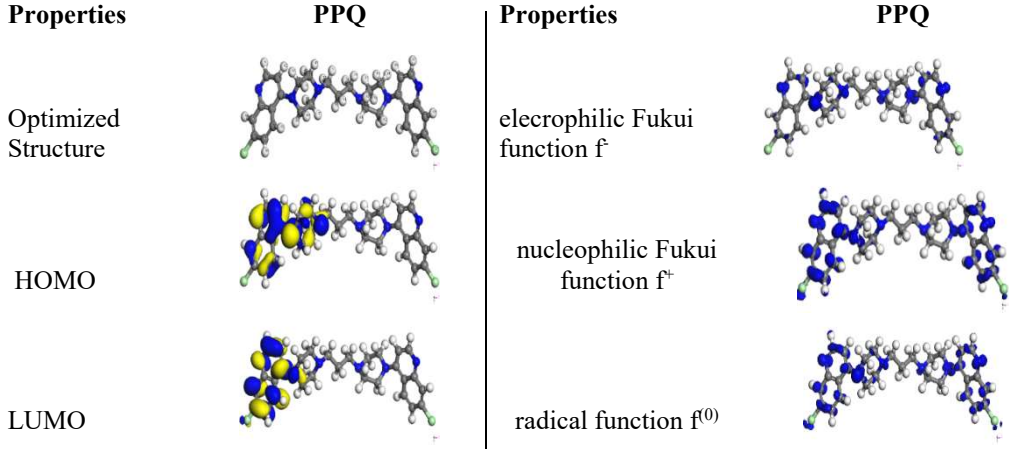

Figure 4: Computational information showing, HOMO, LUMO optimized structures, ω, δ and radial functions for PPQ molecule.

Table 5: Quantum chemical parameters for PPQ.

Inhibitor	E_{HOMO}	E_{LUMO}	ΔE (eV)	IP (eV)	EA (eV)	χ (eV)	η (eV)	σ (eV)	ω (eV)	δ (eV)
PPQ	-3.104	-2.997	0.107	4.110	3.287	3.698	0.412	2.427	16.59	0.060

ΔE value was recorded as 0. 107 (Table 5), indicating a very close molecular interaction between the various energy levels [25-28]. ΔE is the minimum energy required to excite an electron, which is stuck in its bound state, into a free state, where it can participate in a reaction [21-23]. By this definition, ΔE obtained from this experiment shows that PPQ molecules were likely to easily be excited into a free state on the MS surface, hence leading to faster and stronger adsorption and IE(%) [19, 24, 27]. This result was supported by E_{HOMO} higher value (-3.104) than E_{HOMO} (-2.997).
Fig. 4 shows that PPQ is symmetrical. HOMO electron density distribution was deeply located on the double bonds of the aromatic benzene ring and N heteroatoms. LUMO was located on the individual C atoms of the aromatic ring, heteroatoms and Cl atom present as a substituent. PPQ high IE(%) is linked to the donating power of the π-electrons and heteroatoms present in the aromatic ring [28-32]. PPQ had a higher absolute molecular σ and η of 2.4 and 0.4, respectively, which makes it a better CI for MS in $[Na_3H(CO_3)_2]$ heavy deposits [33-36].

Thermodynamics consideration

To access the inhibitor strength in increasing the energy barrier required to be overcome for the corrosion reaction between $[Na_3H(CO_3)_2]$ and MS to occur, Arrhenius Eq. (its plots are shown in Fig. 5) was adopted [16, 21].

$$lnr = lnA - \frac{Ea}{R}\frac{1}{T} \qquad (13)$$

where r is rate and A is collision factor, while other constants remain the same, as conventionally known.

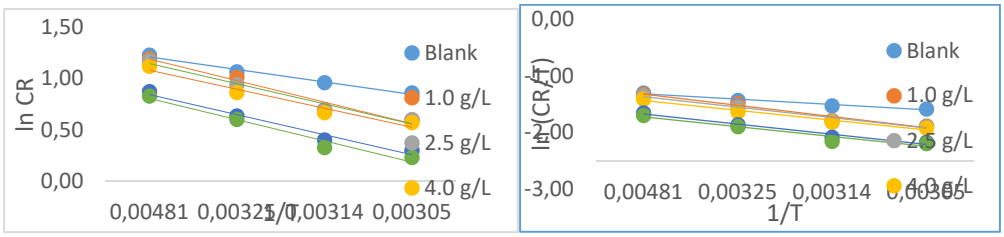

(a) **(b)**

Figure 5: Plots of: **(a)** Arrhenius and **(b)** Eyring for PPQ IE(%) of MS corrosion in $[Na_3H(CO_3)_2]$ deposits.

From Table 6, E_a values in the solution with PPQ were higher than of those without it, and increased with higher Ct, implying that there was a CR slowdown, due to PPQ adsorption, and a likely physical adsorption [22-24, 29]. The transition state Eq. for ΔH and ΔS_{ads} determination is [13, 19, 30]:

$$\ln\frac{k}{T} = -\frac{\Delta H_a}{R}\frac{1}{T} + \ln\frac{kB}{h} + \frac{\Delta S_a}{R} \qquad (14)$$

where k is reaction rate, k_B is the Boltzman constant and h is the plank constant. Table 6 presents negative entropy values, implying an increased inhibition, due to PPQ stronger adsorption onto MS, which resulted from the significant degree of orderliness [31-33]. ΔH_{ads} values that are positive and lower than 80 Kj/mol^{-1} represent a physical adsorption mechanism and an endothermic reaction,

indicating bond breaking around corrosion forming sites [5, 17, 34]. ΔG_{ads} values in Table 6 were negative and lower than -20 $kJmol^{-1}$, implying physical adsorption, spontaneity of reaction and high PPQ stability [22, 33-35]. These results showed strong agreement with gravimetric analysis.

Table 6: Thermodynamic data on PPQ adsorption onto MS in $[Na_3H(CO_3)_2]$ deposits.

Inhibitor C (g/L)	E_a (kJ/mol)	ΔH_{ads} (kJ/mol)	(R^2)	ΔS_{ads} (kJ/mol)
Blank	1.01	78.8	0.9689	-951.5
1.0	1.74	164.6	0.9665	-943.6
2.5	1.63	153.8	0.9813	-948.4
4.0	1.53	143.9	0.9752	-974.5
5.5	1.62	145.6	0.9358	-978.1
7.0	1.23	149.9	0.9981	-984.8

Adsorption consideration

Langmuir's adsorption isotherm was used to test PPQ, to determine its inhibition mechanism. This process was accomplished through Langmuir's plots of Ct/θ *vs*. Ct (g/L) (Fig. 6), using Eq. 10 [6, 18, 34].

$$\frac{Ct}{\theta} = \frac{1}{k} + Ct \qquad (15)$$

Table 7 shows the data obtained from the plots in Fig. 6.

Table 7: Langmuir's isotherm data for PPQ adsorption onto MS in $[Na_3H(CO_3)_2]$ deposits.

T (K)	k (mg/L)	(R^2)	ΔG^*_{ads} (kJ/mol)
208	4.845	0.99	- 9.67
308	2.258	0.99	- 12.37
318	1.904	0.98	- 12.32
328	1.599	0.98	- 12.23

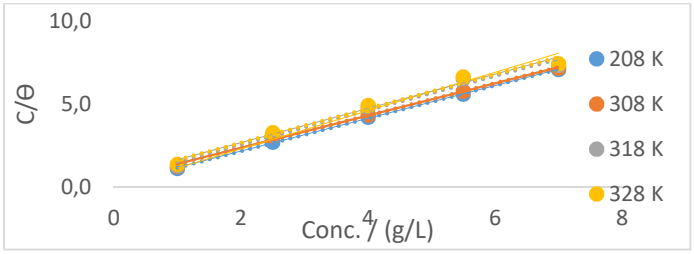

Figure 6: Langmuir's adsorption isotherm plot for PPQ inhibition of S275JR MS corrosion in $[Na_3H(CO_3)_2]$ deposits.

It was observed that k values in the inhibited solution decreased with increased T. This phenomenon is always suggestive of a physical adsorption mechanism, as it was confirmed from the T dependent result (gasometric analysis) [30, 34]. This result also indicates that there was room for a speedy migration of the molecules in the solution, which enabled a strong bond formation between PPQ and MS, hence obeying Langmuir's assumption of monolayer adsorption [14, 19]. ΔG_{ads}

values were negative, and lower than -20 Kj/mol^{-1}, which defines a physical adsorption phenomenon, spontaneity to the forward direction and increased inhibitor stability [35].

SEM analysis

To investigate PPQ nature of adsorption onto MS, SEM was deployed [34-35], through the study of topographic, morphological and compositional information. Fig. 5 shows MS micrographs in blank, 1.0 and 7.0 g/L [$Na_3H(CO_3)_2$. The micrograph in Fig. 7a shows a very rough surface area, which depicts the aggressive attack by the [$Na_3H(CO_3)_2$] solution on MS, due to PPQ absence [35]. This was due to the corrosion sites activation triggered [$Na_3H(CO_3)_2$], which caused MS anodic dissolution and possible cathodic HER [30-31]. However, PPQ lowest Ct gave the micrograph seen in Fig. 7b, which shows a possible decrease in the $R_{a\ of}$ MS. A further increase in the Ct of PPQ (Fig 7c) caused complete MS smoothness. This could be due to the large θ by PPQ of the MS surface, which protected anodic corrosive active sites that could have been open for electrons transfer into [$Na_3H(CO_3)_2$], leading to corrosion [30, 35]. These micrographs show that PPQ is a good inhibitor of MS corrosion in [$Na_3H(CO_3)_2$].

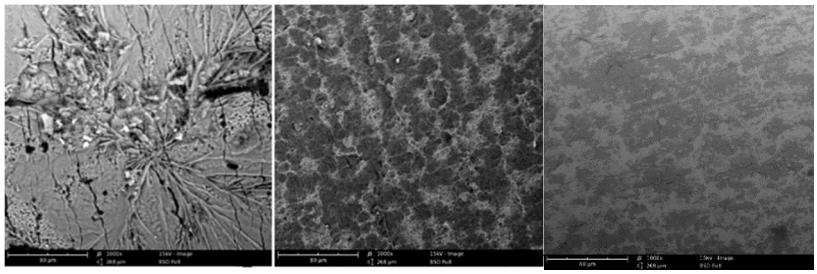

(a) **(b)** **(c)**

Figure 7: Micrographs obtained for CI of MS in: **(a)** [$Na_3H(CO_3)_2$] **(b)** 1.0 g/L and **(c)** 7.0 g/L solution of [$Na_3H(CO_3)_2$].

Conclusion

PPQ as alternative inhibitor showed effective corrosion mitigation of S275JR MS in heavy deposits. IE(%) of 98.8, 99.5, 82.9 and 95.9% were obtained by gravimetric, HER, EIS and PDP, respectively, which makes PPQ a better inhibitor for corrosion deactivation. It had a shortest ΔE of 0.1 Ev, with a molecular σ and η of 2.4 and 0.4, respectively, which makes it a better inhibitor of MS corrosion in [$Na_3H(CO_3)_2$] heavy deposits. PPQ was thermodynamically stable, and had low disorderliness. Its adsorption onto the MS surface was physical and spontaneous. These are qualities that come with a good and reliable inhibitor.

Authors' contributions

B. U. Ugi: designed the research work; carried out data analysis and interpretation; supervised all the work. **V. M. Bassey**: was involved in materials and samples collection and preparation; did the experimental work. **P. B. Ashishie**: was involved in materials and samples collection and preparation. **N. D. Obi**: did experimental work. **F. B. Ugi**: carried out data analysis and interpretation. All authors read and review the manuscript.

Abbreviations
AC: alternating current
$CaCl_2$: anhydrous calcium chloride
C_{dl}: double layer capacitance
CE: counter electrode
CI: corrosion inhibitor/inhibition
CR: corrosion rate
Ct: concentration
E_a: activation energy
EA: electron affinity
Ec: electrochemical
E_{corr}: corrosion potential
E_{HOMO}: energy of the highest occupied molecular orbital
EIS: electrochemical impedance spectroscopy
E_{LUMO}: energy of the lowest unoccupied molecular orbital
i_{corr}: corrosion current density
IE(%): inhibition efficiency
IP: ionization potential
IT: immersion time
k: equilibrium constant values
Mp: melting point
$[Na_3H(CO_3)_2]$: sodium sesquicarbonate
OCP: open circuit potential
PDP: potentiodyamic polarization
PPQ: piperaquine
R_2: correlation coefficient
R_a: surface roughness
R_{ct}: charge transfer resistance
RE: reference electrode
S275JR MS: mild steel
SCE: saturated calomel electrode
SR: scan rate
T: temperature
WE: working electrode
WL: weight loss

Symbols definition
β_a: anodic slope
β_c: cathodic slope
δ: neucleophilicity
ΔE: energy gap
ΔG_{ads}: adsorption free energy
ΔH: heat of adsorption
ΔH_{ads}: enthalpy of adsorption
ΔS_{ads}: entropy of adsorption
η: absolute hardness
θ: surface coverage
σ: absolute softness
χ: absolute electronegativity
ω: electrophilicity index

References

1. Abdallah M, Gad EAM, Sobhi M et al. Performance of tramadol drug as a safe inhibitor for aluminum corrosion in 1.0 M HCl solution and understanding mechanism of inhibition using DFT. Egyptian J Petrol. 2019;(28):173-181. http://doi.org./10.1016/j.ejpe.2019.02.003
2. Agwamba EC, Udoikono AD, Hitler L et al. Synthesis, characterization, DFT studies, and molecular modeling of azo dye derivatives as potential candidate for trypanosomiasis treatment. Chem Phys Impact. 2022;(4)*:*100076 http://doi.org./10.1016/chphi.2022.100076
3. Ameh PO, Eddy NO. Experimental and computational chemistry studies on the inhibition efficiency of phthalic acid (PHA) for the corrosion of aluminum in hydrochloric and tetraoxosulphate (VI) acids. Protec Met Phy Chem Surf. 2018;(2):1-13. http://doi.org./10.1134/S2070205118060035
4. Ammouchi N, Allal H, Belhocine Y et al. DFT computations and molecular dynamics investigations on conformers of some pyrazinamide derivatives as corrosion inhibitors for aluminum. J Mol Liq 2020;(300):112309. http://doi.org./10.1016/j.molliq.2019.112309
5. Bashir S, Sharma V, Kumar S et al. Inhibition performances of Nicotinamide against aluminum corrosion in an acidic medium. Port Electrochim Acta. 2020;(38):107-123. http://doi.org./10.4152/pea.202002107
6. Bai Y, Sui H, Liu X et al. Effects of the N, O, and S heteroatoms on the adsorption and desorption of asphaltenes on silica surface: a molecular dynamics simulation. Fuel. 2019;(240):252-261. http://doi.org./ 10.1061/j.fuel.2018.11.135
7. Bharatiya U, Gal P, Agrawal A et al. Effect of corrosion on crude oil and natural gas pipeline with emphasis on prevention by ecofriendly corrosion inhibitors: a comprehensive review. J Bio-Tribo Corr. 2019;(5):35 http://doi.org./10.1007/s40735-019-0225-9
8. Bhuvaneswari M, Santhakumari R, Usha C et al. Synthesis, growth, structural, Spectroscopic, optical, Thermal, DFT, HOMO–LUMO, MEP, NBO analysis, and Thermodynamic properties of vanillin isonicotinic hydrazide single crystal. J Mol Struct. 2021;(4):130856. http://doi.org./10.1016/j.molstruc.2021.130856
9. Boumhara K, Harhar H, Tabyaoui M et al. Corrosion inhibition of mild steel in 0.5 M H_2SO_4 solution by *Artemisia herba-alba* Oil. J Bio-Tribo Corr. 2019;(5):1-8 http://doi.org./10.1007/s40735-018-0202-8
10. Dagdag O, El Harfi A, Cherkaoui O et al. Rheological, electrochemical, surface, DFT and molecular dynamics simulation studies on the anticorrosive properties of new epoxy monomer compound for steel in 1 M HCl solution. RSC Adv. 2019;(9):4454-4462. http://doi.org./10.1039/c8ra09446b
11. Diki NYS, Coulibaly NH, Kambire O et al. Experimental and theoretical investigations on copper corrosion inhibition by cefixime drug in 1 M HNO3 solution, J Mater Sci Chem Eng. 2021;(9). http://doi.org./10.4236/msce.2021.95002
12. Dimakis N, Salas I, Gonzalez L et al. Li and Na adsorption on graphene and graphene oxide examined by density functional theory, quantum theory of atoms in molecules, and electron localization function. Molecules. 2019;(24):754. http://doi.org./10.3390/molecules24040754

13. Ebenso EE, Verma C, Olasunkanmi LO et al. Molecular modelling of compounds used for corrosion inhibition studies: a review. Phys Chem Chem Phys 2021;(23):19987-20027. http://doi.org./10.1039/D1CP00244A
14. El-Monem MA, Shaban MM, Khalil MMH. Synthesis, Characterization and computational chemical study of Aliphatic Tricationic surfactants for metallic equipment in oil fields. ACS Omega. 2020;(5):26626-26639. http://doi.org./10.1021/acsomega.0c03432
15. Erazua EA, Adeleke BB. A computational study of quinolone derivatives as corrosion inhibitors for mild steel. J Appl Sci Environ Manag. 2019;(23):1819-1824. http://doi.org./10.4314/jasem.v23i10.8
16. Erteeb MA, Ali-Shattle EE, Khalil SM et al. Computationl studies (DFT) and PM3 theories on thiophene oligomers as corrosion inhibitors for iron. Amer J Chem. 2021;(11):1-7. http://doi.org./10.5923/j.chemistry.20211101.01
17. Fajobi MA, Fayomi OSI, Akande IG et al. Inhibitive Performance of Ibuprofen Drug on Mild Steel in 0.5 M of H_2SO_4 Acid. J Bio-Tribo Corr. 2019;(5):1-5. http://doi.org./10.1007/s40735-019-0271-3
18. Fouda AES, El-Askalany AH, Molouk AFS. Experimental and computational chemical studies on the corrosion inhibitive properties of carbonitrile compounds for carbon steel in aqueous solution. Sci Rep. 2021;(11):67-79. http://doi.org./10.1038/s41598-021-00701-z
19. Geerlings P, Chamorro E, Chattaraj PK et al. Conceptual density functional theory: status, prospects, issues. Theor Chem Account. 2020;(139):36. http://doi.org./10.1007/s00214-020-2546-7
20. Hsissou R, Abbout S, Seghiri R et al. Evaluation of corrosion inhibition performance of phosphorus polymer for carbon steel in [1 M] HCl: Computational studies (DFT, MC and MD simulations). J Mater Res Tech. 2020;(9):2691-2703. http://doi.org./10.1016/j.jmrt.2020.01.002
21. Jiajun FU, Su-ning L, Wang Y. Computational and electrochemical studies of some amino acid compounds as corrosion inhibitors for mild steel in hydrochloric acid solution. J Mater Sci. 2020;(45):6255-6265. http://doi.org./10.1007/s10853-010-4720-0
22. Joshi BD, Thakur G, Chaudhary MK. Molecular structure, homo-lumo and vibrational analysis of ergoline by density functional theory. Sci World. 2021;(14):21-30. http://doi.org./10.3126/sw.v14i14.34978
23. Liu Q, Song Z, Han H et al. A novel green reinforcement corrosion inhibitor extracted from waste *Platanus acerifolia* leaves. Const Build Mat. 2020;(260):119695. http://doi.org./10.1016/j.conbuildmat.2020.119695
24. Majda MT, Ramezanzadeh M, Ramezanzadeh B et al. Production of an environmentally stable anti-corrosion film based on *Esfand* seed extract molecules-metal cations: Integrated experimental and computer modeling approaches. J Haz Mat. 2020;(382):1-16. http://doi.org./10.1016/j.hazmat.20192019.121029
25. Onyeachu IB, Abdel-Azeim S, Chauhan DS et al. Electrochemical and Computational insights on the application of expired Metformin drug as a novel inhibitor for the sweet corrosion of C1018 steel. ACS Omega. 2021;(6):65-76. http://doi.org./10.1021/acsomega.0c03364

26. Padash R, Sajadi GS, Jafari AH et al. Corrosion control of aluminum in the solutions of NaCl, HCl and NaOH using 2, 6-dimethylpyridine inhibitor: Experimental and DFT insights. Mat Chem Phys. 2020;(244):122681. http://doi.org./10.1016/j.matchemphys.2020.122681
27. Rbaa M, Ouakki M, Galai M et al. Simple preparation and characterization of novel 8-Hydroxyquinoline derivatives as effective acid corrosion inhibitor for mild steel: Experimental and theoretical studies. Col Surf A: Physicochem Eng Aspects. 2020;(602):125094. http://doi.org./10.1016/j.colsurfa.2020.125094
28. Sharma S, Ganjoo R, Saha SK et al. Experimental and theoretical analysis of baclofen as a potential corrosion inhibitor for mild steel surface in HCl medium. J Adhs Sci Tech. 2021;(1). https://doi.org/10.1080/01694243.2021.200230
29. Solomon MM, Umorena SA, Quraishia MA et al. Effect of akyl chain length, flow, and temperature on the corrosion inhibition 1 of carbon 2 steel in a simulated acidizing environment by an imidazoline-based inhibitor. J Petrol Sci Eng. 2020;(2):1-39. http://doi.org./10.1016/j.petrol.2019/106801
30. Su P, Li L, Li W et al. Expired drug theophylline as potential corrosion inhibitor for 7075 aluminum alloy in 1 M NaOH solution. Int J Electrochem Sci. 2020;(15):1412-1425. http://doi.org./10.20964/2020.02.25
31. Tan J, Guo L, Wu D et al. Electrochemical and computational studies on the corrosion inhibition of mild steel by 1-Hexadecyl-3-methylimidazolium Bromide in HCl medium. Int J Electrochem Sci. 2020;(15):1893-1903. http://doi.org./10.20964/2020.03.36
32. Thanh LT, Vu NSH, Binh PMQ et al. Combined experimental and computation studies on corrosion inhibition of *Houttuynia cordata* leaf extract for steel in HCl medium. J Mol Liq. 2020;(315):113787 http://doi.org./10.1016/j.molliq.2020.113787
33. Ugi BU, Obeten ME, Bassey VM et al. Adsorption and inhibition analysis of aconitine and tubocurarine alkaloids as eco-friendly inhibitors of pitting corrosion in ASTM – A47 low carbon steel in HCl acid environment. Indon J Chem. 2022;(22):1-16. http://doi.org./10.22146/ijc.56745
34. Xi J, Liu C, Morgan D et al. An Unexpected Role of H During SiC Corrosion in Water. J Phys Chem C. 2020;(124):9394-9400. http://doi.org./10.1021/acs.jpcc.0c02027
35. Zaher A, Chaouiki A, Salghi R et al. Inhibition of mild steel corrosion in 1 M hydrochloric medium by the methanolic extract of *Ammi visnaga Lam*. seeds. Hindawi Int J Corr. 2020;(1):1-10. http://doi.org./10.1155/2020/9764206